Unveiling the effect of magnetite on the synergistic action of deposits and microorganisms on carbon steel corrosion

Maria A. Diaz-Mateus, Laura L. Machuca, Hanan Farhat, Silvia J. Salgar-Chaparro

Corrosion Science 231 (2024) 111940

Contents lists available at ScienceDirect

Corrosion Science

journal homepage: www.elsevier.com/locate/corsci

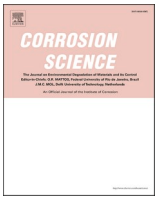

Unveiling the effect of magnetite on the synergistic action of deposits and microorganisms on carbon steel corrosion

Maria A. Diaz-Mateus [a], Laura L. Machuca [b], Hanan Farhat [c], Silvia J. Salgar-Chaparro [a,*]

[a] Curtin Corrosion Centre, WA School of mines: Minerals, Energy and Chemical Engineering, Curtin University, Bentley, WA, Australia
[b] WA School of Mines: Minerals, Energy, and Chemical Engineering, Curtin University, Bentley, WA, Australia
[c] Qatar Environment & Energy Research Institute (QEERI), Doha, Qatar

ARTICLE INFO

Keywords:
Microbiologically influenced corrosion
Magnetite
Oilfield-recovered consortium
Under deposit corrosion
Synergistic corrosion
Carbon steel

ABSTRACT

The synergistic corrosion effect of microorganisms and deposits on carbon steel corrosion was assessed with magnetite and sand. In the presence of the microbial consortium with magnetite, uniform corrosion rates were 3.5 times higher (0.611 mm/year) than the sum of the corrosion rates promoted by the consortium and deposit separately (0.056 and 0.110 mm/year, respectively). Conversely, with sand, uniform corrosion rates were only 1.5 times higher (0.093 mm/year) than the sum of the corrosion rates promoted by the consortium and deposit separately (0.056 and 0.006 mm/year, respectively). The heightened synergistic effect is attributed to magnetite's semi-conductive nature.

1. Introduction

Microbiologically influenced corrosion (MIC) is renowned for causing severe localised corrosion across various industrial sectors, including oil and gas, healthcare, transportation, shipping, mining, and food processing [1–3]. The corrosion initiated or sustained by microorganisms and their metabolisms accounts for approximately 20% of the total corrosion costs [4,5], which, according to a NACE International study, amounted to nearly US$2.5 trillion in 2016 [6]. Despite significant multidisciplinary research contributions from fields such as electrochemistry, chemical engineering, microbiology, and corrosion engineering, several knowledge gaps remain concerning the underlying processes and factors contributing to MIC [7]. Addressing these knowledge gaps has proven challenging, partly due to the complexity of replicating all the factors and conditions present in real-world environments. Laboratory investigations of MIC often fail to replicate field conditions, which may include intricate multispecies consortia, shear stress, traces of chemical treatments, high pressure, and salinity, and the presence of scales, corrosion products, and deposits. Consequently, replicating such conditions in laboratory-based experimentation can be logistically impractical and may introduce undesirable experimental variables while attempting to address specific research questions.

In operational oil and gas pipelines, corrosion products, mineral scales, and silica sands tend to accumulate on the internal surfaces of the pipes. Particularly at the 6 o'clock position and inclined sections such as elbows [8]. Findings from both laboratory investigations and field cases indicate that these deposits pose a threat to pipeline integrity, as they lead to a form of localised corrosion known as under-deposit corrosion (UDC) [8]. In such scenarios, microorganisms can colonise these deposits and accelerate metal deterioration by disrupting passivating oxides, converting protective oxide layers into less effective ones, and forming new oxide layers [9]. This combined action of microorganisms and deposits on metal corrosion has been observed in field and laboratory scenarios [10–12]. Moreover, this phenomenon is commonly reported in pipe corrosion failure analyses [13–15] and has recently been termed under deposit microbial corrosion (UDMC). A term defined as "electrochemical, physical, and microbiological processes compromising pipeline integrity" [16].

From a MIC perspective, it is suggested that in the context of UDMC, deposits facilitate microorganism colonization, offering protection from the shear stress present in pipelines, thereby increasing the risk of MIC, i.e., the presence of deposits intensifies the likelihood of MIC. From the UDC perspective, the proposition is that, in UDMC scenarios, the accumulation of microorganisms beneath the deposits heightens the heterogeneity of these deposits. This accumulation gives rise to concentration cells of corrosive metabolic by-products, culminating in a more severe manifestation of UDC. The lack of integration of both corrosion phenomena has led to inaccurate diagnoses and

* Corresponding author.
E-mail address: silvia.salgar@curtin.edu.au (S.J. Salgar-Chaparro).

https://doi.org/10.1016/j.corsci.2024.111940
Received 9 October 2023; Received in revised form 18 January 2024; Accepted 20 February 2024
Available online 23 February 2024

underestimation of this type of corrosion. We propose that UDMC poses a higher corrosion risk for carbon steel than UDC alone and MIC in isolation. This heightened risk is attributed to a synergistic corrosion effect. Consequently, studies focused on UDC must incorporate the presence of microorganisms in their experimental protocols. To the best of the author's knowledge, only the study conducted by Yang et al., [17] has demonstrated that the combined presence of a silica sand deposit and *Desulfovibrio desulfuricans* results in a higher corrosion rate than either of them could cause individually, thus exhibiting synergistic corrosion on carbon steel.

Despite the prevalence of magnetite (Fe_3O_4) as a deposit in oil and gas pipelines, the majority of studies focussing on the effect of microorganisms on under-deposit corrosion (UDC) have predominantly used inert deposits such as sand and clay [18,19]—this prevalent choice of inert deposits for research warrants reconsideration. Magnetite stands out as the predominant corrosion product identified in the analysis of ruptured pipelines. Notably, it can enter these systems as residual mill scale from tube manufacturing and storage or form a corrosion byproduct under conditions of limited oxygen availability [20]. Furthermore, due to its superior electrical conductivity and nobility compared to carbon steel in the electrochemical series, magnetite is recognised for its potential to initiate galvanic corrosion when unevenly distributed across metal surfaces [21–23]. Simultaneously, magnetite has gained increased attention in MIC research due to its role in facilitating extracellular electron transfer (EET) [24]. EET is a microbial strategy that enables electron transfer between microorganisms and solid materials, such as naturally occurring metal compounds [25]. It plays a key role in a microbial corrosion mechanism known as Electrical MIC (EMIC), where microorganisms directly adsorb electrons from elemental metallic iron, using it as their electron donor [26]. EMIC has been identified as the cause of pit depths as high as 17 μm in carbon steel after a 7-day incubation period [27]. A recent study with *Geobacter sulfurreducens* demonstrated that the addition of magnetite doubled the current densities recorded in the presence of the biofilm alone. The authors suggested that magnetite can facilitate EET from the stainless steel (Fe^0) into the biofilm, similar to the outer-surface c-type cytochrome OmcS [28]. Therefore, it is imperative to incorporate magnetite more frequently in laboratory-based UDMC studies to generate more accurate risk assessments of this type of corrosion.

In real-world field conditions, the coexistence of magnetite as corrosion product or deposit and native microorganisms is widespread. Consequently, quantifying the risk of corrosion under the synergistic effect of magnetite and microorganisms is of great significance. Based on the above introduction, it is reasonable to hypothesise that magnetite could amplify the potential synergistic corrosion effect of deposits and microorganisms on carbon steel compared to an inert deposit. Biostatistics, surface analysis, bioinformatics tools, and microbial data were employed to assess whether and why magnetite and microorganisms can synergistically affect to a higher extent the corrosion of carbon steel.

2. Materials and methods

2.1. Oilfield microbial consortium

The microbial consortium used in this study was recovered from a sand deposit collected from a High-pressure (HP) separator in an Australian oil production facility experiencing MIC. The consortium was maintained in a synthetic produced water of the following composition: 212.5 mM NaCl, 7.43 mM $CaCl_2{\cdot}2\ H_2O$, 5 mM KCl, 27.4 mM $MgCl_2{\cdot}6\ H_2O$, 0.04 mM SrCl·6 H_2O, 10 mM D-glucose, 13.8 mM $Na_2SO_4{\cdot}5\ H_2O$, 11.3 mM $Na_2S_2O_3{\cdot}5\ H_2O$, 1.54 mM $NaHCO_3$, 26 mM Na-formate, 26 mM Na-lactate, 20 mM Na-acetate, 12.4 mM NH_4NO_3, 1.3 g L^{-1} casamino acids (Bacto™), and, 1 L of ultrapure water (Milli-Q system, resistivity 18.2 MΩ·cm). The pH was adjusted to 7.2 ± 0.2 using a 100 mM sodium hydroxide solution. The synthetic solution was poured in Hungate tubes under a 99.9% N_2 gas atmosphere and sterilised by autoclaving at 121°C for fifteen minutes at 208 kPa. One gram of field sand was inoculated in the tubes and incubated at 40°C for 20 days. After incubation, an aliquot from the inoculated solution was transferred to a fresh synthetic solution prior to the experiment to establish the microbial consortium.

2.2. Mineral deposit characterisation

Commercial magnetite (Fe_3O_4) and silicon dioxide (SiO_2) from Sigma-Aldrich were used in the corrosion experiments. Sand and magnetite particle size was determined by laser diffraction analysis, and specific surface area was measured by the Brunauer, Emmett, and Teller (BET) method; results are given in Table 1. Both deposits were sterilised by autoclaving at 134°C for three minutes at 208 kPa prior to the experimental setup.

2.3. Evaluation of the synergistic effect of magnetite and microorganisms on carbon steel corrosion

2.3.1. Carbon steel sample preparation

Carbon steel 1030 grade used for corrosion experiments had the following chemical composition (weight %): C (0.30), Mn (0.69), Si (0.24), S (0.030), P (0.010), Cr (0.022), Ni (0.001), Mo (0.001), Cu (0.005), and Fe (balance). The samples were laser-cut into rectangular coupons with 12 ×22×9 mm thick dimensions and electro-coated with an inert epoxy resin (Powercron 6000CX, PPG Industrial coatings). The top face of each rectangular sample was wet-ground to a 600-grit finish using silicon carbide paper to limit the working surface area (2.6 cm^2). All samples were washed with ethanol, weighted, and sterilised by UV radiation for 15 min prior to the experiment setup.

2.3.2. Experimental conditions

To determine the synergistic action of deposits and microorganisms on carbon steel corrosion, two distinct sets of experiments were conducted, each outlined as follows:

Experiment 1: Magnetite, a semi-conductive deposit was used in immersion tests, exploring two conditions: 1) Magnetite (M): Carbon steel exposed to magnetite. 2) Magnetite + Consortium (M + C): Carbon steel with magnetite and the microbial consortium.

Experiment 2: Sand, an inert deposit, was used in immersion tests, with two conditions studied: 1) Sand (S): Carbon steel immersed in the sand; 2) Sand + Consortium (S + C): Carbon steel in the sand with the microbial consortium.

A control test was included in both experiments, Blank (B): Carbon steel without magnetite and microbial consortium. Additionally, a biotic control was tested to assess the microbial consortium's influence on MIC, Consortium (C): Carbon steel exposed only to the microbial consortium.

This structured approach allowed us to thoroughly determine whether the corrosion rates generated by the simultaneous presence of deposits and microorganisms were higher than the sum of the corrosion rates caused individually by the deposit and by the microbial consortium. And to compare the synergistic corrosion effect with sand against magnetite. Moreover, the height and weight of the deposit used were controlled by placing 3.8 g of each commercial deposit on the prepared sample, previously positioned in a rectangular 3D-printed epoxy box. The custom-made epoxy sample holder was designed to allow the deposition of 10 mm of mineral powder on top of the metal (Figure S1).

Table 1
Deposits characterization.

Model deposit	Mean particle size (μm)	Specific surface area (m^2/g)
Magnetite (Fe_3O_4)	4.67	5.41
Sand (SiO_2)	4.55	6.48

The above immersion tests were conducted using a test solution with the same composition described in Section 2.1. Anaerobic conditions were maintained in the reactors throughout the 22-day exposure time by continuous injection of N_2 gas (20 mL/min). Agitation and a constant solution temperature of 40 ºC were achieved using a stirring hotplate set to 200 rpm. In the reactors including microorganisms (biotic), continuous nutrient replenishment was performed using a 5 L reservoir glass cell connected to a peristaltic pump. The pump was calibrated to replace 30% of the reactor solution in each reactor every 24 hours.

2.3.3. Reactors monitoring

Microbial metabolism was monitored throughout the immersion period. Secondary metabolites (nitrates and sulphide) present in the test solution were measured every five days using spectrophotometry (Hach™, DR3900). The concentration of total dissolved iron (FeT) was measured by the USEPA FerroVer® method following the manufacturer's instructions. The Methylene Blue Method and the Ferrous Sulphate Method were used for the determination of sulphide and nitrites, respectively. The test solution pH was measured using a portable pH meter (Thermo Scientific™, Star A221).

2.3.4. Corrosion measurements

After immersion, corrosion analyses were performed on triplicate coupons from each experimental condition. The metal surface was cleaned using Clark's solution, as described in the ASMT G1 Standard [29]. Corrosion rates in mm/year were calculated based on mass loss, steel density, immersion time, and exposed surface area [29]. Surface analysis was performed on the same triplicate coupons using a 3D surface profilometer (Solarius™, SolarScan) with a spot size of 10–100 μm and resolution of 0.2 μm. The 3D inspection system is equipped with SolarScan NT software version 7.4. Profile analysis involved measuring step height to determine the maximum pit depth on each coupon. The pitting rate was calculated by dividing the deepest pit in mm by the exposure time in days, as described in the NACE SP0775 standard practice [30].

2.3.5. Surface morphology

Carbon steel coupons were subjected to scanning electron microscopy imaging using a field emission scanning electron microscope (FESEM, Tescan Clara) to visually examine and compare the corrosion damage after immersion.

2.4. Cross-section profiles of surface corrosion products

For a comprehensive characterisation of the subsurface structures near the metal and the corrosion products formed under each condition, cross-sectional analysis was conducted using FESEM coupled with energy-dispersive X-ray spectroscopy (EDS). The metal coupons were mounted in epoxy resin (EpoFix), and the cross-sections were prepared by grinding and polishing steps until a final polishing of 1 μm finish with diamond suspension. The samples were coated with a platinum layer (10 nm thick) to increase surface electric conductivity. Surface analysis was performed using a FESEM (Tescan Clara), with images collected at 20 kV using the backscatter detector. Data analysis was conducted using Aztec 3.0 software (Oxford Instruments NanoAnalysis).

2.5. Influence of magnetite-deposit presence on the cross-section profiles of sessile microbial communities

While sessile populations (biofilms) in direct contact with metallic surfaces are known to mediate most of MIC [31], the microbial attributes of sessile microorganisms developed within the bulk deposits were also analysed. Examining the microbial community differences between populations in direct contact with the metal and those formed within the deposits will provide insights into how microorganisms spatially interact with deposits and how they influence corrosion. Details are given in the sections below.

2.5.1. Viability of sessile microorganisms

To assess the viability of sessile microorganisms developed on the bare metal, at the deposit-metal interphases in the deposited samples, and within the bulk of the deposits, three coupons from each biotic reactor were removed at the end of the exposure. These samples were gently immersed in a sterile phosphate-buffered saline (PBS) solution to remove planktonic cells. Carbon steel samples without deposits were immediately placed in Falcon tubes containing 10 mL of PBS solution with Tween 20 (0.1% w/v final concentration). The bulk of the deposits was separated from the carbon steel sample using a sterile scalpel blade (Figure S2). Afterward, the bulk deposit and the covered carbon steel coupons were also placed in Falcon tubes containing 10 mL of PBS solution with Tween 20 (0.1% w/v final concentration). Sessile bacteria were detached from the carbon steel and bulk deposit by sonication, as described elsewhere [32].

An aliquot of 1 mL of the PBS solution containing the sessile microorganisms was inoculated into 9 mL of fresh test solution (See Section 2.3.2.) and serially diluted 10-fold in triplicate for the most probable number (MPN) estimation. The serial dilutions were incubated at 40 ºC for 20 days, and microbial growth was determined to be positive based on visually noticeable changes in the turbidity and colour of the culture media. The microbial concentration was calculated using the MPN 3-tube standard table [33]. Sessile bacteria counts were expressed as cells per cm^2 of the surface area of the metal coupon (cells/cm^2) or cells per gram of deposit (cells/g). The remaining 9 mL of PBS solution containing detached cells was used for further microbiological analyses.

2.5.2. Adenylate energy charge estimation

The physiological status of the sessile microbial communities developed on the bare carbon steel, bulk deposit, and at the deposit-metal interphase in biotic test with both deposits was determined by measuring the intracellular concentrations of adenosine triphosphate (ATP), adenosine diphosphate (ADP), and adenosine monophosphate (AMP). The AXP assay and the Quench-Gone Organic Modified (QGO–M) test kits (LuminUltra™) were employed for this purpose, according to the manufacturer's instructions. The concentrations of these adenosine nucleotides in the PBS solution containing the detached sessile microorganisms were determined by luminescence using a luminometer (LuminUltra™, PhotonMaster) after reaction with the luciferin-luciferase enzyme. Adenylate energy charge (AEC) was calculated according to the following formula:

$$AEC = (ATP+0.5ADP)/(ATP+ADP+AMP) \quad (1)$$

2.5.3. Microbial community composition

Next-generation sequencing of the 16 S rRNA gene from DNA and RNA molecules was used to characterise the sessile communities [34]. The microbial cells were detached from the solid matrix using sonication as described elsewhere [32]. After sonication, the cell suspension was centrifuged at 15,000x g for 5 min at 4°C for pelleting the cells and preserved at –80°C until nucleic acid extraction.

a) Nucleic acid extraction: Simultaneous DNA and RNA extraction was conducted using the Norgen DNA/RNA/Protein kit (Norgen Biotek Corp) following the manufacturer's procedures. Total DNA was eluted in 100 μL of nuclease-free water, and total RNA was eluted in 50 μL of nuclease-free water. DNA concentration was verified using a spectrophotometer (Thermo Scientific™, NanoDrop Lite). Following RNA extraction, genomic DNA was removed from the samples using the Turbo DNA-free kit (Invitrogen) according to the manufacturer's instructions. RNA was then purified using an RNeasy MinElute cleanup kit (Qiagen) and transcribed into complementary DNA

(cDNA) using the SuperScript IV first-strand synthesis system (Invitrogen), as described previously [35].

b) Library preparation and sequencing: The eluted DNA and synthetised cDNA were used as templates for amplification of the V3-V4 hypervariable region of the 16 S rRNA gene [36]. Sequencing was conducted by the Marshall Centre at the University of Western Australia (UWA) using next-generation paired-end sequencing on a sequencing instrument (Illumina, MiSeq).

c) Bioinformatics analysis: Raw FASTQ files were demultiplexed and assigned to respective samples based on their unique barcodes by the Marshall Centre. Demultiplexed sequences from each sample were trimmed and quality-filtered using the "dada2 denoise-paired" plugin on the Quantitative Insights Into Microbial Ecology Software (QIIME 2) [37]. The DADA2 quality settings "- -p-trunc-len-f 280" and "- -p-trunc-len-r 220" were applied to truncate the forward and reverse sequences at 280 and 220 positions, respectively. The QIIME 2 feature-classifier plugin was used to classify the representative sequences against a pre-trained SILVA database, generating the taxonomy table [38]. The taxonomy table was visualised with R-studio.

2.6. Statistical analysis

Statistical analysis of corrosion and pitting data was conducted using SPSS 27 and PAST (V4.10). The choice of statistical analyses depended on the normality of the data for each variable. The Shapiro-Wilk method was used to test the normality of the data for each variable. Subsequently, one-way analysis of variance (ANOVA) with Tukey's post-hoc means separation test was implemented to test the homogeneity of variances in each variable and identify statistically significant differences between normally distributed variables. The results of statistical tests were considered significantly different when the p-value was $\leq$ 0.05.

3. Results

3.1. Changes in water chemistry throughout exposure

Fig. 1 shows the pH and concentrations of total sulphides (H_2S, HS^-), nitrites (NO_2^-), and total dissolved iron in the test solution for the different experimental scenarios and throughout the exposure. Fig. 1A, 1B and 1C indicate that nitrites, dissolved iron, and sulphide concentrations in the biotic tests were consistently higher than those in the abiotic tests throughout the immersion period. These results suggest, together with the blackening of the test solution and the strong H_2S smell in the gas outlet of the setup indicate, that the microbial consortium carried out sulphate/thiosulphate reduction and nitrate reduction [39]. Moreover, their metabolism was having an impact on the corrosion of carbon steel.

Notably, the concentration of sulphides and nitrites in biotic conditions with deposits significantly differed from those without deposits, likely due to the establishment of distinct microbial community structures in each condition (See Section 3.7.). Intriguingly, conditions without deposits, B, and C showed higher levels of dissolved iron in the test solution compared to their respective abiotic and biotic counterparts. These results provide insights into two potential phenomena: 1) The deposits protected the metal from corrosion, resulting in no iron presence in the bulk solution. 2) The deposits served as diffusion barriers, impeding the movement of Fe^{+2} from the corroding metal to the bulk solution. The pH of the test solution became more alkaline over time in all six scenarios due to the continuous N_2 saturation.

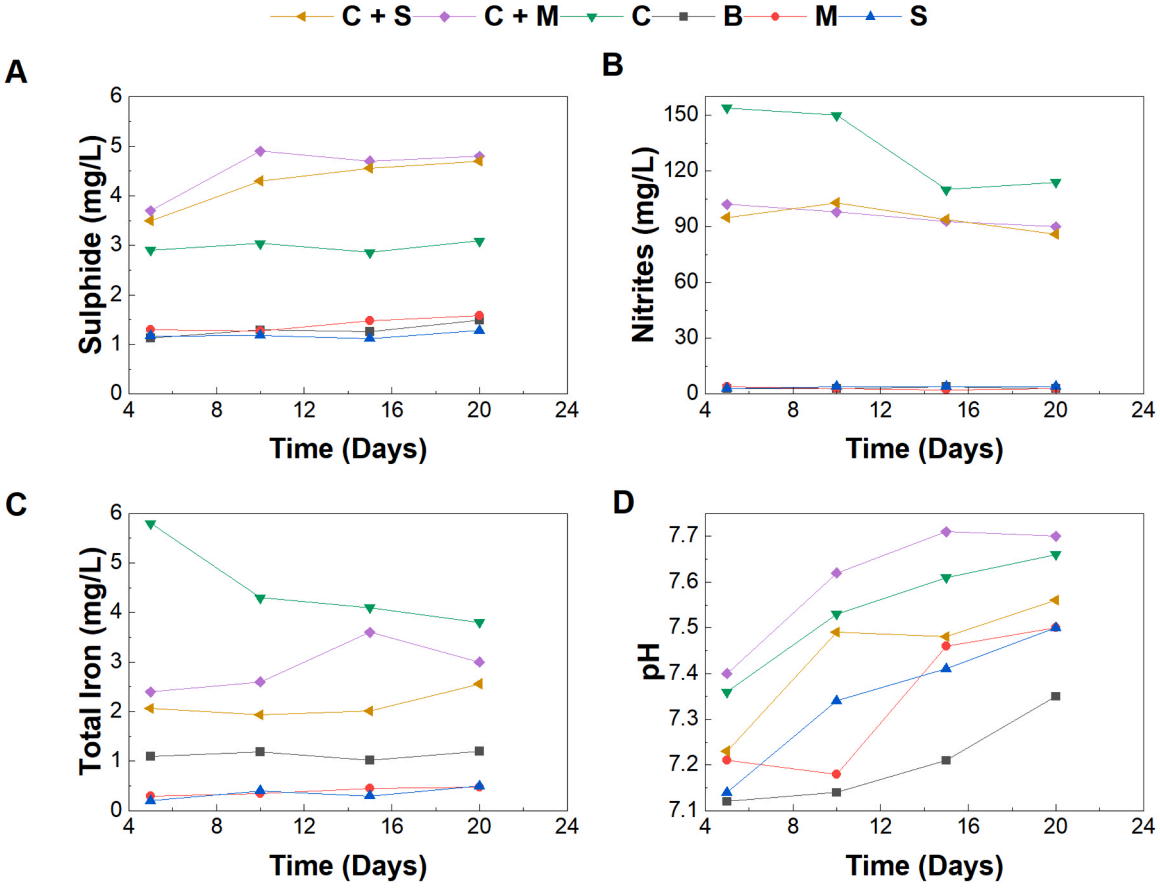

Fig. 1. Test solution chemical monitoring over time. A. Dissolved sulphides (H_2S, HS^-) B. Dissolved nitrites (NO_2^-) C. Total dissolved iron D. pH.

3.2. Corrosion measurements

3.2.1. Corrosion rates

The average corrosion rates under the six different scenarios are shown in Fig. 2A. In the absence of deposits and microorganisms in the solution (Blank), the corrosion rate was 0.022 mm/year. In the presence of sand deposits without bacteria, the corrosion rate decreased to 0.006 mm/year, whereas in the presence of magnetite, the corrosion rate increased to 0.110 mm/year. Statistically significant differences were observed in the corrosion rates between those three scenarios (M, B, and S) ($p \leq 0.05$, Table S1). These results suggest that sand alone hinders the uniform corrosion of carbon steel, and magnetite alone accelerates it.

In the experimental condition with the microbial consortium alone (C), the measured corrosion rate was 0.056 mm/year. However, in the combined presence of the consortium and magnetite (C+M), the corrosion rate increased to 0.611 mm/year. Notably, the synergistic effect of the microbial consortium and magnetite in C+M yielded a corrosion rate 3.6 times higher than the sum of the individual corrosion rates promoted by C and M (0.166 mm/year). These findings establish a clear synergistic corrosion effect between the microbial consortium and magnetite on carbon steel. Similarly, when the microbial consortium was accompanied by sand (C+S), the corrosion rate (0.093 mm/year) was 1.5 times higher than the sum of the individual corrosion rates promoted by C and S (0.062 mm/year). These results confirm the synergistic corrosion effect between the microbial consortium and sand on carbon steel, too. Moreover, the corrosion rates in the presence of deposits and microorganisms (C+S and C+M) were significantly higher compared to their abiotic counterparts (S and M, respectively) with a *p*-value of ≤ 0.05 (Table S1), demonstrating that UDMC is greater than UDC for both sand and magnetite deposits.

Concurrently, the average corrosion results validate the role of deposits as diffusion barriers proposed in Section 3.1. Despite reactor B exhibiting the highest total dissolved iron concentrations throughout the test compared to reactors M and S, it did not register the highest average corrosion rates among the abiotic reactors. Similarly, reactor C did not exhibit the highest corrosion rates among the biotic reactors, yet it had the highest concentrations of dissolved iron throughout the test. Consequently, there appears to be no direct correlation between dissolved iron concentration and corrosion rates, indicating that the presence of deposits hindered the flow of Fe^{+2} from the metal-deposit interface to the solution.

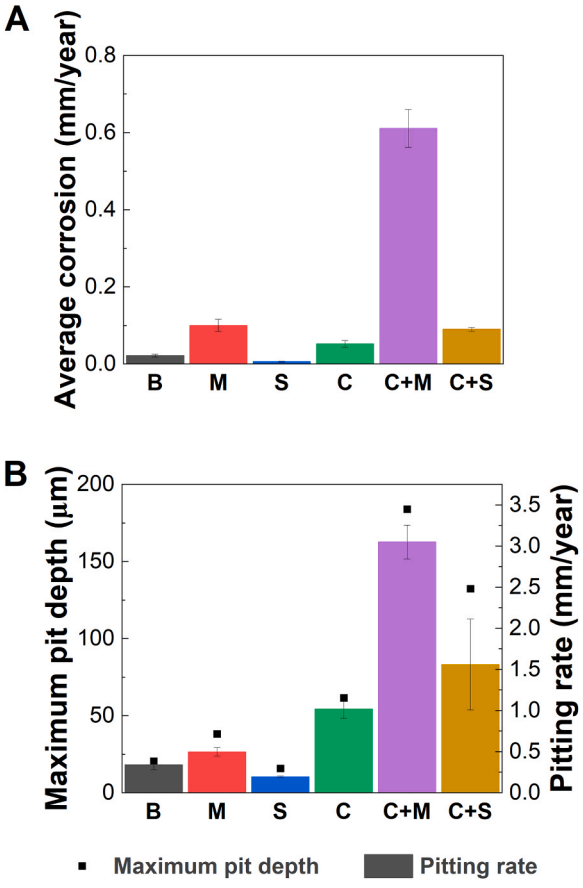

Fig. 2. Corrosion rates were calculated after immersion in six different conditions. A. Average corrosion rates calculated based on weight loss. B. Pitting rates calculated based on the deepest pit on the working surface.

3.2.2. Pitting corrosion

Surface profilometry was conducted to measure the depth of pits formed on the exposed surface of the carbon steel coupons; results are shown in Fig. 3. Carbon steel exposed to the microbial consortium and magnetite exhibited the most severe localised corrosion (Fig. 3D). Interestingly, different corrosion patterns were observed across the different biotic scenarios: Fig. 3B shows small pits and large cavities that may have formed from coalesced pits in the metal surface exposed to the microbial consortium alone. Fig. 3D shows localised corrosion in the form of large wide cavities on the metal coupon exposed to magnetite and the microbial consortium. Fig. 3F depicted severe pitting corrosion in the form of small pits distributed throughout the sample on the metal exposed to sand and the microbial consortium.

Pitting rates were calculated based on the deepest observed points. Across the six assessed conditions, pitting rates exhibited a parallel trend to the uniform corrosion rates (Fig. 2B): the pitting rate was 0.326 mm/year in the blank condition (B), decreased to 0.193 mm/year in the presence of the sand deposit (S), and increased to 0.495 mm/year in the presence of the magnetite deposit (M). These findings reinforce the observations regarding uniform corrosion, emphasising that sand may hinder pitting, while magnetite, when present alone, accelerates pitting. However, it is worth noting that no statistically significant differences were detected among the pitting rates in the abiotic scenarios (see Table S2).

The pitting rates observed in the reactor with metal exposed solely to the microbial consortium (C) was 1.019 mm/year. However, when the microbial consortium was accompanied by magnetite (C+M), the pitting rate increased to 3.340 mm/year. These results indicate that the corrosion rates caused by the synergism of microorganisms and magnetite were 2.2 higher than the pitting rates obtained when the corrosion rates promoted by C alone and M alone are added separately (1.519 mm/year). This underscores the synergistic corrosion effect of the microbial consortium on carbon steel in the presence of magnetite. Similarly, when the microbial consortium was accompanied by sand (C+S), the pitting rate was 1.557 mm/year, a pitting rate 1.2 higher than the sum of the rates promoted by C alone and S alone 1.212 mm/year). This indicates a synergistic corrosion effect of the microbial consortium on carbon steel in the presence of sand, albeit causing less severe metal damage.

The pitting rates and average corrosion rates (Fig. 2A) obtained in this study highlight that both sand and magnetite deposits enhance MIC and consequently demonstrate that UDMC leads to higher corrosion than UDC with this specific microbial consortium.

3.3. SEM analysis of carbon steel samples

SEM images of the metal surfaces exposed to different conditions exhibited varying morphologies (Fig. 4). The blank carbon steel surface appeared uniform, with visible grinding marks, indicating low average corrosion (Fig. 4A). However, pits were observed on the surface, suggesting that localised damage was greater than uniform damage in the samples, which aligns with the corrosion measurements shown in Fig. 2.

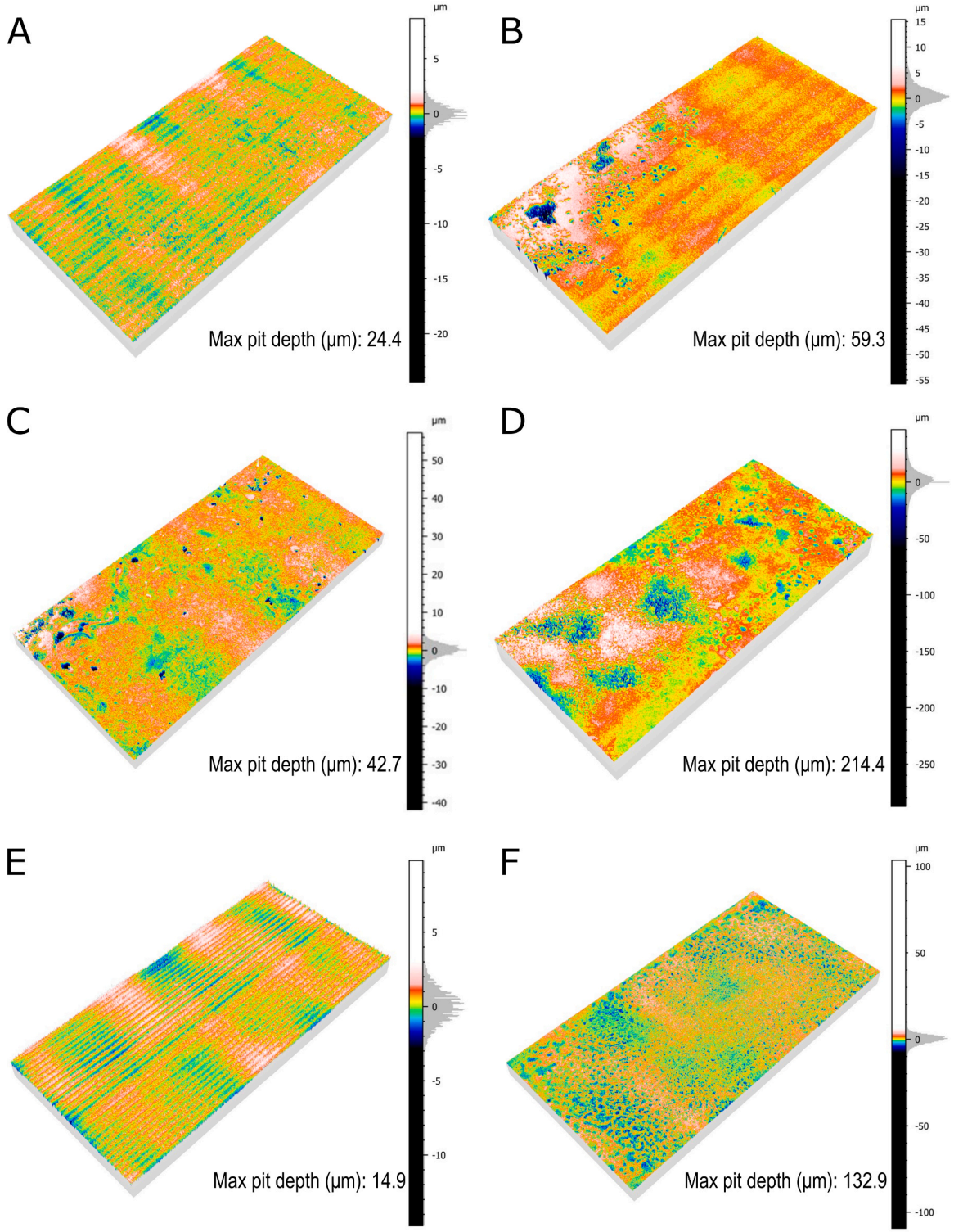

Fig. 3. Surface profilometry of carbon steel exposed to six different experimental scenarios. A. Metal sample exposed to the test solution (Blank). B. Metal sample exposed to the microbial consortium (C). Metal sample exposed to magnetite (M). D. Metal sample exposed to the microbial consortium and magnetite (C+M). E. Metal sample exposed to sand (S). F. Metal sample exposed to the microbial consortium and sand (C+S).

In the presence of magnetite (Fig. 4B), the coupon surface was rougher than in the blank condition, indicating increased uniform damage. The galvanic coupling between the semiconductor magnetite deposit and the carbon steel surface likely contributed to the enhanced metal damage compared to the blank condition (Fig. 4A) and to the coupon exposed to sand (Fig. 4C) [21]. The carbon steel coupon exposed to the sand deposit alone appeared generally smooth, with visible grinding marks from the sample preparation process, and showed minimal pitting corrosion (Fig. 4C). Figs. 4D, 4E, and 4F account for the metal samples exposed to the microbial consortium, magnetite, and sand, respectively. Overall, rougher surfaces were observed compared to their abiotic counterparts, showing the effect of microorganisms on the severe deterioration of the metal. Fig. 4E exhibited wider and darker pits, suggesting greater pit depths. Fig. 4F displayed numerous tinny pits with a morphology similar

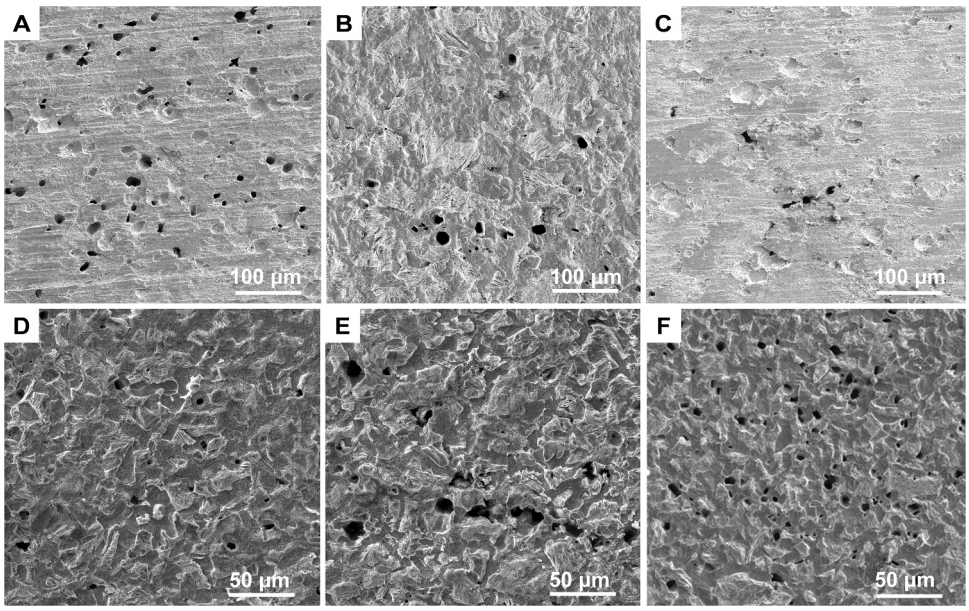

Fig. 4. SEM analysis of carbon steel coupons after immersion (corrosion products removed): A. Metal sample exposed to the test solution (Blank). B. Metal sample exposed to magnetite (M). C. Metal sample exposed to sand (S). D. Metal sample exposed to the microbial consortium (C). E. Metal sample exposed to the microbial consortium and magnetite (C+M). F. Metal sample exposed to the microbial consortium and sand (C+S).

to those in Fig. 4D but with a higher quantity compared to the other two metals exposed to biotic conditions, consistent with the profilometry images shown in Fig. 3.

3.4. Cross-sectional analysis of metal-deposits interphase

SEM-EDS images of the cross-sections of metal samples under biotic conditions are presented in Fig. 5. The corrosion layer surface in the deposited samples, whether magnetite or sand (Figs. 5B, 5C), appears continuous and flat. In contrast, the surface of the corrosion products in the bare sample (Fig. 5A) appears uneven, porous, or multi-layered. This difference may be attributed to the additional weight of the deposit later on top of the corrosion products, resulting in a more organised and compact distribution. A significant attack can be observed in the transition from the corrosion product layer to the metal in all biotic conditions, a phenomenon not observed in samples immersed under abiotic conditions (Figure S3).

The corrosion product elemental composition in direct contact with the carbon steel, across all test scenarios (biotic and abiotic), primarily comprised oxygen and iron (Fig. 5 and Figure S3). Nevertheless, a distinct sulphur layer was evident in coupons exposed to the microbial consortium alone (Fig. 5A) and in conjunction with magnetite (Fig. 5B), and in metal samples exposed to sand and magnetite (Figure S3). It is important to highlight that sulphur compounds were detected in the test solutions of all experiments through chemical monitoring (See Section 3.1); however, EDS analysis identified a sulphur layer in only select scenarios. This discrepancy may be attributed to the limitation of only one cross-sectional analysis per condition.

In the coupons exposed to both magnetite deposit and the microbial consortium (Fig. 5B), distinct accumulations of chlorine and oxygen became apparent within specific sections of the corroded area. A discernible sulphur layer was also observed, separating the bulk magnetite deposit from the corroded metal. Moreover, the overlapping signals of iron, sulphur, and oxygen in the bulk magnetite indicate the formation of iron sulphide (FeS) within the magnetite deposit. A notable divergence in the EDS cross-sectional analysis between the condition with both magnetite and microorganisms (C+M) and its abiotic control (M) was the thinner sulphur layer observed in the abiotic condition (M), with no discernible accumulation of chlorine on the metal surface (see Figure S3A).

Similarly, EDS analysis of the sample exposed solely to the microbial consortium (Fig. 5A) revealed a predominant iron signal in the upper layer of the corrosion products, followed by an almost continuous and intense sulphur layer. A lower-intensity iron signal accompanied the sulphur layer, suggesting the presence of FeS in this section. Notably, sodium and oxygen were found to accumulate in the corroded areas. In the elemental map of the cross-sectioned metal exposed to the microbial consortium and sand deposit, a high signal of oxygen and iron was exclusively detected within the corroded areas. Meanwhile, silicon, oxygen, and sulphur signals overlapped within the bulk sand, again suggesting the formation of FeS throughout the sand deposit.

3.5. Microbial viability

The MPN of sessile microorganisms found under the two deposits, on the bare metal, and in the bulk sand and magnetite, are presented in Table 2. The concentration of sessile microorganisms developed on the bare metal (C) after 22 days of immersion is four orders of magnitude higher (1.1×10^{9} cells/cm^2) than the sessile bacteria developed under the sand and magnetite deposits after the same immersion period (4.6×10^{5} and 1.2×10^{5} cells/cm^2, respectively). Moreover, similar cell concentrations were measured in the samples directly interacting with the test solution: C, Bulk magnetite, and Bulk sand. These findings suggest that the 10 mm deposit layer (either sand or magnetite) significantly influenced the mass transfer processes of the nutrients available in the test solution. Sessile microorganisms at the metal-deposit interphase could only obtain limited nutrients, leading to lower microbial growth.

3.6. Microbial activity

Adenylates estimation was performed to determine the differences in the physiological state and stress levels of sessile communities formed under the two deposits and on the bare metal surface. AEC values were also determined for the sessile communities developed within the two model deposits. AEC values higher than 0.8 typically correspond to metabolically active microbial populations. Stressed but viable populations (i.e., in a stationary growth phase) typically have AEC values

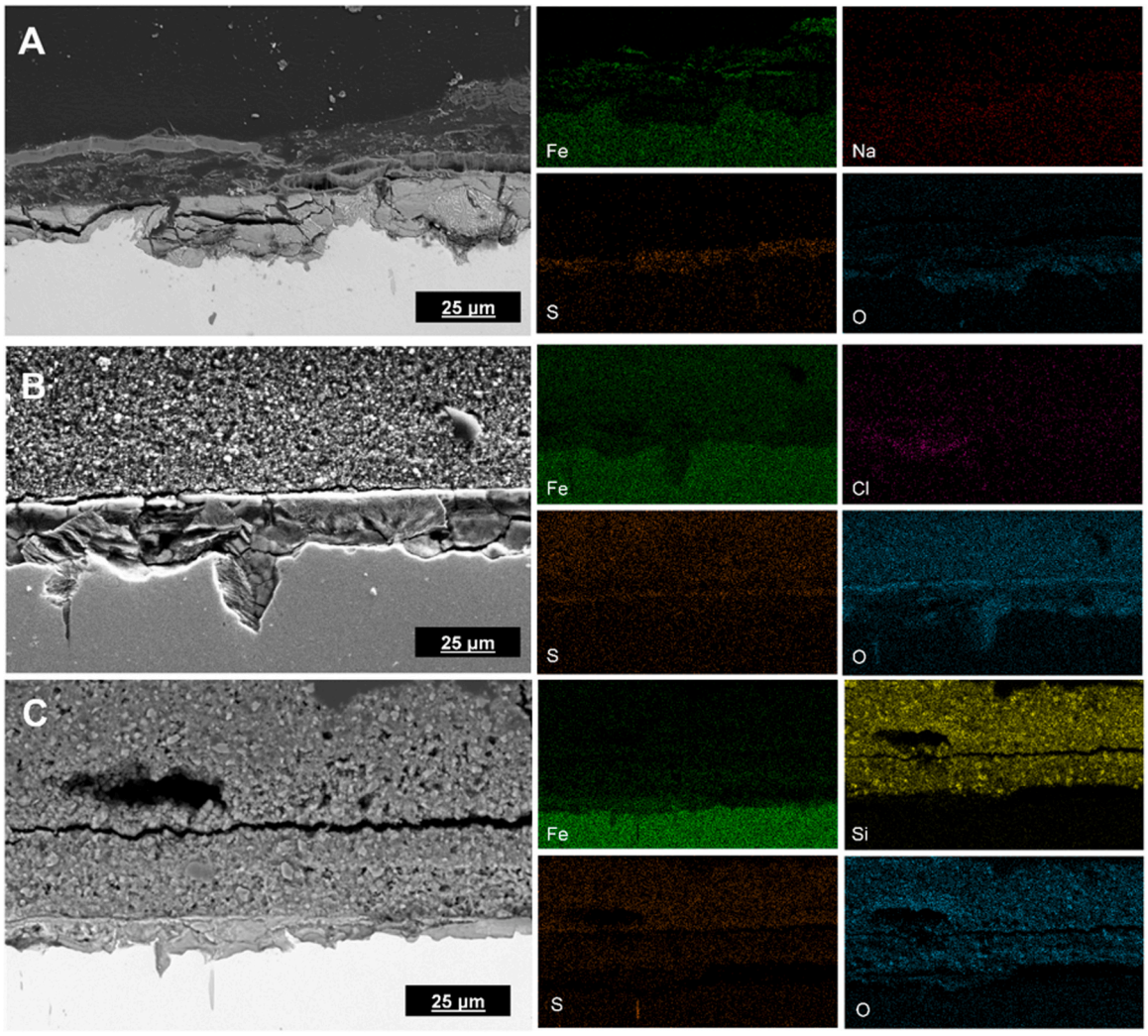

Fig. 5. SEM-EDS imaging of cross-sectioned coupons exposed to three different biotic conditions for 22 days. A. Metal coupon exposed to the microbial consortium (C). B. Metal coupon exposed to the microbial consortium and magnetite (C+M). C. Metal coupon exposed to the microbial consortium and sand (C+S).

Table 2
Cell concentrations of sessile microorganisms formed in the different experimental conditions.

Reactor	Section	MPN (cells/cm^2) or (cells/g)	95% Confidence limits	
			Lower	Higher
C	Bare metal	1.1×10^9	1.8	41
C + M	Bulk deposit	1.1×10^9	1.8	41
	Deposited metal	1.1×10^5	0.17	1.8
C + S	Bulk deposit	1.1×10^9	1.8	41
	Deposited metal	4.6×10^5	0.90	20

between 0.5 and 0.8, while senescent populations have AECs lower than 0.5 [40].

The AEC ratios measured in each tested condition are presented in Fig. 6. The highest AEC was found in the sessile population growing in the bare metal (1.0) in the absence of deposits and in direct contact with the test solution. The microbial populations formed under the 10 mm layer of sand and magnetite were stressed (viable but not actively growing), with AEC ratios of 0.8 and 0.5, respectively. However, a significant difference was observed in the AEC ratios of the sessile population formed within the sand deposit and the one developed within the magnetite deposit (bulk deposit). Sessile microorganisms interacting

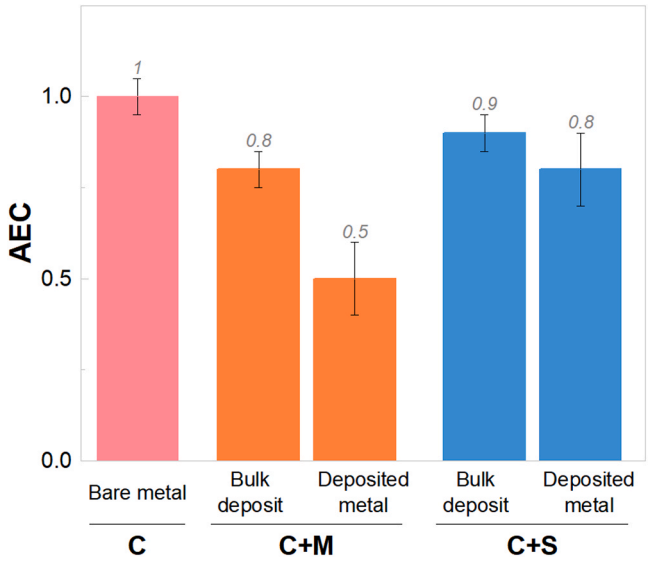

Fig. 6. AEC ratios of the sessile populations formed on deposited metal (under sand and magnetite deposits) and bare metal after immersion.

with the magnetite (despite showing higher microbial concentration than sand, Table 2) were in a stationary growth phase or viable (AEC of 0.8). In contrast, the sessile bacteria interacting with sand were actively growing (AEC of 0.9).

3.7. Microbial community composition

DNA and RNA-based amplicon sequencing identified total and active sessile microorganisms developed on the bare metal and bulk magnetite deposits. A total of 959,555 high-quality sequences were obtained after bioinformatics processing of the raw data. Fig. 7 displays the taxonomic distribution of sessile populations and the percentage of their relative abundance in each experimental scenario.

The molecular analysis of microorganisms in each experimental condition revealed consistent dominance by *Tepidibacillus* sp. and *Pseudomonas* sp., accompanied by a lower proportion of *Bacillus* sp. (Fig. 7). In the total microbial communities, *Pseudomonas* sp. constituted the majority (88.20%) in the absence of deposits. Conversely, within magnetite and sand environments, *Tepidibacillus* sp. prevailed, accounting for 50.33% and 72.3% of the total communities, respectively. The highest percentage of *Bacillus* sp. in the total communities was observed in the presence of magnetite (C+M).

When examining metabolically active populations based on RNA analysis, *Pseudomonas* sp. was the most active member (91.48%) in the absence of deposits. In the presence of magnetite, *Pseudomonas* sp. was the most active species (52.06%) despite *Tepidibacillus* sp. being the most abundant. Conversely, in sand-deposited samples, *Tepidibacillus* sp. dominated the total community and constituted the dominant taxa in the active community. The highest proportion of *Bacillus* sp. in the active communities was again observed in the presence of magnetite (C+M).

Furthermore, diversity profiling analysis highlighted variations in sessile bacterial community composition in response to environmental conditions, including the presence or absence of deposits and the deposit type.

4. Discussion

4.1. Corrosion behaviour in the presence of magnetite alone – Reactor M

The results presented in this study demonstrate that the presence of a 10 mm layer of magnetite deposited on carbon steel (M) significantly increased (five times) the uniform corrosion rates of carbon steel compared to the Blank condition (B). The qualitative categorisation of the corrosion rates changed from low to moderate, according to the NACE SP0775 standard [30]. This finding aligns with previous reports that have shown magnetite to considerably accelerate carbon steel corrosion, particularly galvanic corrosion, in both aerated and deaerated systems [21,22,41,42].

Magnetite is a semiconductor corrosion product with a more noble potential than steel. Consequently, when coupled with carbon steel, it acts as a cathode [43]. Hence, it is plausible to assert that in test M, the magnetite layer coupled with the carbon steel. Due to its powder nature, an uneven deposit layer was deposited on the metal surface, and microanodic zones were likely created in the areas where magnetite was not in direct contact with the metal. Meanwhile, the magnetite layer represented a large cathodic area [22]. This hypothesis gains further support from the fact that the sole distinguishing factor between the magnetite deposit and the sand deposit is their electrical conductivity. The particle size and surface area of both sand and magnetite were similar (Table 1), and laboratory-based studies have consistently shown that these two properties can significantly impact the severity of corrosion induced by deposits [44,45].

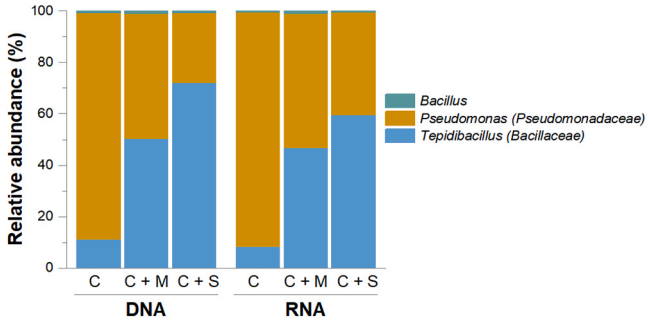

Fig. 7. Relative abundance of total and active sessile microorganisms formed on bare, sand-deposited, and magnetite-deposited carbon steel after immersion. Each bar represents the results from the three replicates evaluated in each condition.

Simultaneously, elemental composition analysis of the compounds present at the magnetite-metal interphase, obtained with EDS (Figure S3B), revealed a continuous thin layer of oxygen immediately on top of the metal sample, with a thinner sulphur layer underneath. Iron oxides and iron sulphides were likely formed abiotically on the exposed carbon steel surface, as O and S overlap with Iron. The measured concentration of sulphides in the M test during the test solution monitoring (Fig. 1) supports this finding. Previous research has demonstrated that even low concentrations of sodium thiosulphate (as low as 0.01 M) can facilitate the formation of iron sulphides (FeS) on carbon steel surfaces through disproportionation/reduction reactions in chlorine-rich solutions [46,47]. Furthermore, FeS has been identified as a factor contributing to galvanic corrosion on carbon steel by also acting as a cathode for the anodic dissolution of metal (Eq. (7), resulting in corrosion rates as high as 6 mm/year [48,49].

Based on the above, the reactions of the proposed corrosion mechanism evidenced in the presence of magnetite and the absence of bacteria (Reactor M, Fig. 2) are as follows:

Reactions in the anodic region:

$$Fe \rightarrow Fe^{2+} + 2e^{-} \quad (2)$$

Reactions in the cathodic region:

$$2H^{+} + 2e^{-} \rightarrow H_2 \quad (3)$$

Reactions for the corrosion products formation are as follows:

$$Fe^{2+} + 2OH^{-} \rightarrow Fe(OH)_2 \quad (4)$$

$$3Fe(OH)_2 \rightarrow Fe_3O_4 + H_2 + 2H_2O \quad (5)$$

$$Fe^{2+} + HS^{-} \rightarrow FeS + H^{+} \quad (6)$$

$$Fe^{0} + 2H^{+} \xrightarrow{FeS} Fe^{2+} + H_2 \quad (7)$$

Iron oxidation of carbon steel (Eq. 2) takes place in the micro anodes of bare metal, whereas the reduction of the dissociated (free) hydrogen ions occurs in the magnetite or cathode (Eq. 3). The released Fe^{+2} ions at the steel surface diffuse, and the corrosion products that these ferrous ions could form will depend on the surrounding pH, dissolved oxygen, and the concentration of environmental ions. Fe^{+2} ions might have combined with the OH^{-} ions released at the cathode to form the first corrosion product (Eq. 4) [50,51]. As solid Iron (II) hydroxide, $Fe(OH)_2$, starts to precipitate at a pH above 6, it is proposed as one of the corrosion products formed in our system [52]. Once $Fe(OH)_2$ is formed, it could have been easily oxidised to form intermediate iron oxides such as magnetite (Eq. 5) [42]. Fe^{+2} ions released during iron oxidation might have also reacted with the elemental sulphur generated from the sodium thiosulphate dissolution in water to form FeS (Eq. 6) [46]. Iron sulphides potentially catalysed the reduction of H^{+} ions to H_2 (Eq. (7). Confirmation of the proposed corrosion mechanism in Reactor M requires further investigation.

4.2. Corrosion behaviour in the presence of the microbial consortium alone – Reactor C

The corrosion test evaluating the effect of the microbial consortium alone (in the absence of deposits) on metal deterioration revealed that microorganisms significantly enhanced the uniform and localised corrosion of carbon steel after 22 days of immersion, as shown in Figs. 2, 3, and 4, compared to the Blank condition. Nevertheless, statistically significant differences were observed only in comparing biotic and abiotic pitting rates, as indicated in Table S2. The addition of the microbial consortium led to a shift in pitting rates from high in the Blank condition to severe in the presence of microorganisms, according to the NACE SP0775 standards [31]. This phenomenon is commonly observed in studies on MIC, as most microbial corrosion mechanisms result in a localised attack on the metal surfaces, which is underestimated when considering only uniform corrosion rates based on weight loss.

The predominant microorganism identified in the biofilms formed on the metal surface was *Pseudomonas* sp. The association of the *Pseudomonas* genus with corrosion processes has been reported in numerous studies [53–56]. Species belonging to this genus are commonly found in natural environments and are considered ubiquitous in oil pipelines [57]. *Pseudomonas* is known for its ability to form slime and develop biofilms that create differential aeration cells in aerobic environments. The areas within the biofilm where low partial pressures of oxygen are trapped act as anodes, while regions with higher oxygen content act as cathodes [58]. Moreover, *Pseudomonas* species have been found capable of corroding carbon steel through extracellular electron transfer (EET), facilitating the transfer of electrons from the extracellular oxidised metal to the interior of the cell for the reduction of oxygen (in aerobic environments) and other oxidants such as sulphate and nitrate (in anaerobic conditions) [55]. Recent studies have also reported that, under anaerobic conditions, *Pseudomonas* causes corrosion of carbon steel by coupling the extracellular oxidation of iron from the metal surface using nitrate as a terminal electron acceptor [53,59].

In addition to *Pseudomonas* sp., the biofilms in condition C also contained *Tepidiobacillus* sp. and *Bacillus sp.*, which accounted for 11 and less than 1% of the abundance, respectively. *Tepidiobacillus* belongs to the *Bacillaceae* family and has been isolated from groundwater [60] or structures in contact with groundwater [61,62]. For this, members of the *Tepidiobacillus* genus are expected to have adapted to extreme environments and exhibit versatile physiology. Species within this genus are moderately microaerophilic, thermophilic bacteria capable of utilizing various terminal electron acceptors such as iron oxides (ferrihydrite, lepidocrocite), transition metals, nitrate, sulphur, and thiosulphate while utilizing different organic and inorganic substrates as the electron donors [60–63]. While limited literature is available regarding the metabolic capabilities of the *Tepidibacillus* genus, no corrosion studies report its contribution to any corrosion process. Note that, contrary to the *Tepidibacillus* genus, the *Bacillus* genus has been reported to contribute to corrosion processes. However, its low abundance in the microbial community makes its participation in the corrosion observed in reactor C very unlikely.

Considering that *Pseudomonas* sp. was the predominant species in both the total and active communities (Fig. 7), it is plausible to attribute the MIC rates of carbon steel in this condition to the activities of this genus. The highest concentrations of nitrites and dissolved iron were found in test C during the test solution monitoring (Fig. 1), indicating that *Pseudomonas* sp. was likely engaged in iron oxidation coupled with nitrate reduction, a thermodynamically favourable corrosion reaction [59]. This reaction includes several metabolic pathways, some of which are described as follows [64]:

$$NO_3^- + 2e^- + 2H^+ \rightarrow NO_2^- + H_2O \quad (8)$$

$$NO_3^- + 8e^- + 10H^+ \rightarrow NH_4^+ + 3H_2O \quad (9)$$

$$2NO_3^- + 10e^- + 12H^+ \rightarrow N_2 + 6H_2O \quad (10)$$

Nevertheless, it is important to highlight that the concentrations of dissolved sulphides in Reactor C, when compared against abiotic controls and the blackening of the test solution, also indicate sulphate/thiosulphate reduction in the presence of the microbial consortium alone. Given the potential of both *Tepidibacillus* and *Pseudomonas* to utilise sulphate/thiosulphate as electron acceptors, the production of H_2S (Eqs. 11 and 12) represents an additional MIC mechanism in Reactor C. However, it is important to note that its impact is considered to be lesser than that of nitrate reduction.

$$Fe^0 + H_2S \rightarrow FeS + H_2 \quad (11)$$

$$Fe^0 + 2H^+ \xrightarrow{FeS} Fe^{2+} + H_2 \quad (12)$$

4.3. Corrosion behaviour in the presence of magnetite and the microbial Consortium – Reactor C+M

This study's results clearly demonstrated a synergistic corrosion effect between deposits and microorganisms for both sand and magnetite. However, this effect was significantly more pronounced with magnetite. Despite similar concentrations of corrosive metabolites (sulphides and nitrites) observed throughout the immersion period (Fig. 1), comparable microbial concentrations at the metal-deposit interphase (Table 2), and similar microbial community structures (Fig. 7) between C+M and C+S, the acceleration of uniform corrosion and pitting rates was notably less pronounced in the presence of inert sand (Figs. 2,3, and 4). This phenomenon can be attributed, in part, to the tendency of microorganisms to exacerbate pre-existing corrosion mechanisms or amplify baseline corrosion processes, clearly evident beneath the magnetite deposit but absent beneath the sand deposit (Fig. 2).

The magnification of magnetite-induced baseline corrosion by the microbial consortium is linked to the generation of corrosive metabolites during microbial metabolic activities. Chemistry monitoring of Reactor C+M revealed the microbial consortium's involvement in both nitrate and sulphate/thiosulphate reduction (Figs. 1A, 1B). During sulphate/thiosulphate reduction, bacteria generate hydrosulphide ligand HS^-, which undergoes a reaction with H^+ to form H_2S. H_2S is known to rapidly react with metallic iron to form the corrosion product iron sulphide (Eq. 11) [65]. Similarly, during nitrate reduction, bacteria produce nitrites (as indicated by Eqs. 8, 9, and 10), and the accumulation of high concentrations of nitrites on the metal surface can decrease the corrosion potential and induce the formation of pits [66,67].

In addition to the corrosion promoted by the microbial consortium corrosive metabolites, it is essential to consider the plausible role of magnetite in facilitating EET [26,28] and, consequently, EMIC. EET is an important biological activity observed in many microorganisms isolated from environments typically deficient in organic electron donors but rich in inorganic substrates, such as mining sites, groundwater, marine sediments, and hydrothermal fields [68–70]. It has been proposed as an adaptive microbial response to obtain energy in organic-poor anaerobic environments and outcompete others for organic electron donors [71]. In our study, the lower AEC of sessile bacteria at the metal-deposit interphase than those on the bulk deposit (Fig. 6) likely resulted from challenging conditions created beneath the 10 mm magnetite layer, hindering optimal microbial development. Microbial EET has been associated with stressful conditions such as the presence of heavy metals [72], extreme pH conditions [73], and carbon source starvation [74], some of which might have occurred under the magnetite. In this scenario, magnetite could have established a connection between microbial cell walls and the metal surface that acted as an electron donor under starvation conditions, i.e., Magnetite may have facilitated the use of Fe^0 as an electron donor while utilizing sulphate and nitrate as final electron acceptors for microbial metabolism.

The low microbial concentrations observed at the metal deposit

interphase of magnetite and sand compared with those in the bulk deposits (Table 2) also support the hypothesis of magnetite facilitating EMIC. Previous reports have shown that EET supports cell maintenance but not cell growth (i.e., cell replication) in anaerobic environments with limited carbon sources [71,75,76]. Since both microbial communities (C+M and C+S) were exposed to starvation under a deposit, both likely engaged in EET. However, the microbial cells under sand limited the number of cells involved in EET to those in direct contact with the metal, while in C+M, magnetite even facilitated the use of Fe^0 as an electron donor for cells located within the magnetite deposit, which were distant from the metal.

Based on the above, the proposed corrosion mechanism in the magnetite-microbial scenario can be summarised as follows:

1) Once the *Tepidibacillus*, *Pseudomonas*, and *Bacillus* sp. biofilm were established at the metal deposit interphase, their metabolic activities led to the formation of corrosive metabolites, including nitrites, organic acids, and hydrogen sulphide, which accumulate at the metal surface due to the diffusion barrier created by the magnetite. EDS-SEM results suggest the formation of iron oxides, iron sulphides, and iron species containing chloride at the metal-deposit interphase (Fig. 5).

2) Nutrients from the bulk were likely unable to reach the biofilm at the metal-deposit interphase, again due to the diffusion barrier presented by the magnetite and nutrient consumption by the sessile bacteria in the top layer of the magnetite bulk deposit (Table 2). This finding is supported by the AXP results (Fig. 6), which indicate high stress levels in the sessile microorganisms in close contact with the metal.

3) Under starvation conditions, the biofilm may have switched its metabolic activity to EET processes [75], facilitated by the presence of magnetite as an electron transfer mediator [26,28,77–79].

Overall, EMIC, chemical MIC, and abiotic corrosion mechanisms may collectively and simultaneously have resulted in the formation and propagation of severe pitting and uniform corrosion rates in the presence of magnetite. The reactions involved in this proposed corrosion mechanism are summarised in Fig. 8.

5. Conclusions

The effect of magnetite in the synergistic action of an oilfield-recovered multispecies consortium and deposits on carbon steel corrosion against sand was investigated. The main findings of the study are as follows:

a. Corrosion testing demonstrated a synergistic corrosion effect between the oilfield-recovered multispecies consortium and deposits, including magnetite and sand. In the presence of these deposits, uniform corrosion and pitting rates were significantly higher than the sum of the rates promoted by the consortium alone, and the deposit (M or S) alone.
b. The synergistic corrosion effect between the microbial consortium and deposits was significantly more severe in the presence of magnetite than sand. This difference occurred despite both scenarios having similar concentrations of corrosive metabolites throughout the immersion period, comparable microbial concentrations at the metal-deposit interphase, and similar microbial community structures.
c. Uniform corrosion and pitting rates revealed that magnetite induced carbon steel corrosion and pitting under abiotic conditions. In contrast, inert sand did not exhibit any corrosion effect. While the electrical conductivity of magnetite was not measured, its semiconductive nature is likely the contributing factor to this phenomenon.
d. Although the exact mechanism underlying the stimulatory effect of magnetite on the synergistic effect of deposits and microorganisms in carbon steel corrosion cannot be definitively proven, it can be partially attributed to the role of microorganisms in accelerating the baseline abiotic corrosion and pitting process initiated by magnetite. Furthermore, the high stress levels measured through the AEC ratio, associated with low microbial cell concentrations beneath deposits, suggest the creation of an environment conducive to EET processes. Considering prior research that has demonstrated magnetite's ability to accelerate EET processes, it is plausible that EMIC also contributed to the observed severe synergistic corrosion effect in C+M.
e. The 16 S rRNA profiling, based on DNA and RNA molecules, demonstrated that microbial communities responded distinctly to the presence or absence of deposits and the type of deposit present in each scenario. These findings emphasize the significant impact of deposit presence on microbial colonization and community composition.

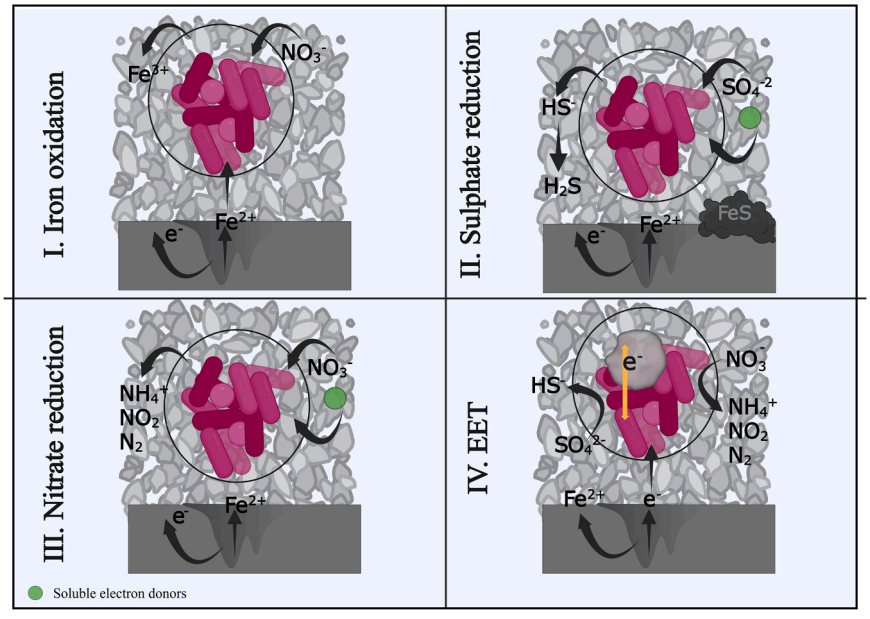

Fig. 8. Schematic illustration of synergistic corrosion of carbon steel in the presence of the microbial consortium and a magnetite deposit. It should be noted that the processes depicted could occur concurrently on corroding metal surfaces; however, they vary in terms of their rates and respective contributions to corrosion.

Funding source

The authors declare that Qatar Environment and Energy Research Institute (QEERI) contributed financial resources to assist this work via a postgraduate scholarship. The study sponsor has reviewed and approved the submission of the manuscript for publication.

CRediT authorship contribution statement

Laura L. Machuca: Writing – review & editing, Supervision, Funding acquisition, Conceptualization. **Hanan Farhat:** Writing – review & editing, Supervision, Funding acquisition. **Maria A. Diaz-Mateus:** Writing – original draft, Methodology, Investigation, Formal analysis, Data curation, Conceptualization. **Silvia J. Salgar-Chaparro:** Writing – review & editing, Supervision, Project administration, Investigation, Conceptualization.

Declaration of Competing Interest

The authors declare that they have no known competing financial interests or personal relationships that could have appeared to influence the work reported in this paper.

Data Availability

Data will be made available on request.

Acknowledgements

The authors acknowledge the financial support from the Qatar Environment and Energy Research Institute (QEERI) for the QEERI - Curtin University Corrosion Center Research Alliance and the Microbiologically Influenced Corrosion (MIC) - Joint Industry Project (JIP) "Preventing and Managing Microbiologically Influenced Corrosion in the Oil and Gas Industry.". Additionally, the authors acknowledge the use of the Microscopy & Microanalysis Facility in the John de Laeter Centre (JDLC) at Curtin University, whose instrumentation has been partially funded by the University, State, and Commonwealth Governments.

Authors statement

MD-M, SS-C, LM conceived and designed the experiments. MD-M carried out the experiment and analysed the data. SS-C, LM, and HF supervised the findings of this work. MD-M prepared the manuscript with input from all authors.

Appendix A. Supporting information

Supplementary data associated with this article can be found in the online version at doi:10.1016/j.corsci.2024.111940.

References

[1] R. Jia, D. Yang, D. Xu, T. Gu, Mitigation of a nitrate reducing Pseudomonas *aeruginosa* biofilm and anaerobic biocorrosion using ciprofloxacin enhanced by D-tyrosine, Sci. Rep. 7 (1) (2017) 6946.
[2] K.M. Usher, A.H. Kaksonen, I. Cole, D. Marney, Critical review: microbially influenced corrosion of buried carbon steel pipes, Int. Biodeterior. Biodegrad. 93 (2014) 84–106.
[3] R. Jia, Y. Li, H.H. Al-Mahamedh, T. Gu, Enhanced biocide treatments with D-amino acid mixtures against a biofilm consortium from a water cooling tower, Front. Microbiol. 8 (2017) 1538.
[4] D. Xu, J. Xia, E. Zhou, D. Zhang, H. Li, C. Yang, et al., Accelerated corrosion of 2205 duplex stainless steel caused by marine aerobic *Pseudomonas aeruginosa* biofilm, Bioelectrochemistry 113 (2017) 1–8.
[5] R. Jia, D. Wang, P. Jin, T. Unsal, D. Yang, J. Yang, et al., Effects of ferrous ion concentration on microbiologically influenced corrosion of carbon steel by sulfate reducing bacterium *Desulfovibrio vulgaris*, Corros. Sci. (2019) 127–137, 153.
[6] Koch, G., Varney, J., Thompson, N., Moghissi, O., Gould, M., Payer, J. (2016). International Measures of Prevention, Application, and Economics of Corrosion Technologies Study. CORROSION 2016 CONFERENCE & EXPO, Houston, TX.
[7] N. Kip, J.A. Van Veen, The dual role of microbes in corrosion, ISME J. 9 (3) (2015) 542–551.
[8] B. Brown, J. Moloney, Under-deposit corrosion, in: A.M. El-Sherik (Ed.), Trends in Oil and Gas Corrosion Research and Technologies, Woodhead Publishing, Sawston, 2017, pp. 363–383.
[9] B.J. Little, T.L. Gerke, R.I. Ray, J.S. Lee, The mineralogy of microbiologically influenced corrosion. Mineral Scales and Deposits, Elsevier, 2015, pp. 107–122.
[10] L.L. Machuca, K. Lepkova, A. Petroski, Corrosion of carbon steel in the presence of oilfield deposit and thiosulphate-reducing bacteria in CO_2 environment, Corros. Sci. 129 (2017) 16–25, https://doi.org/10.1016/j.corsci.2017.09.011.
[11] E.M. Suarez, K. Lepková, M. Forsyth, M.Y. Tan, B. Kinsella, L.L. Machuca, In situ investigation of under-deposit microbial corrosion and its inhibition using a multi-electrode array system, Front. Bioeng. Biotechnol. 9 (2022) 803610.
[12] C. Okoro, S. Smith, L. Chiejina, R. Lumactud, D. An, H.S. Park, et al., Comparison of microbial communities involved in souring and corrosion in offshore and onshore oil production facilities in Nigeria, J. Ind. Microbiol. Biotechnol. 41 (4) (2014) 665–678.
[13] T. Esan, S.D. Kapusta, M.J.J. Simon-Thomas, Case Study: Extreme Corrosion of A 20 Oil Pipeline in the Niger Delta Region, CORROSION, Houston, TX, 2001.
[14] A.K. Samant, S.K. Singh, Role of Microbial Induced Corrosion in Subsea Water Pipeline Failure, CORROSION, San Diego, CA, 1998.
[15] P. Bruijnen, W. van Strien, S. Doddema, Integrated approach toward diagnosing microbiologically influenced corrosion in the petroleum industry, SPE Prod. Oper. 35 (01) (2020) 037–048.
[16] E. Suarez, K. Lepkova, L. Machuca Suarez, The role of bacteria in under-deposit corrosion in oil and gas facilities: a review of mechanisms, test methods and corrosion inhibition, Corros. Mater. 44 (1) (2019) 80–87.
[17] J. Yang, Z.B. Wang, Y.X. Qiao, Y.G. Zheng, Synergistic effects of deposits and sulfate reducing bacteria on the corrosion of carbon steel, Corros. Sci. 199 (2022) 110210.
[18] E.M. Suarez, K. Lepkova, B. Kinsella, L.L. Machuca, Aggressive corrosion of steel by a thermophilic microbial consortium in the presence and absence of sand, Int. Biodeterior. Biodegrad. 137 (2019) 137–146.
[19] H. Liu, G. Meng, W. Li, T. Gu, H. Liu, Microbiologically influenced corrosion of carbon steel beneath a deposit in CO_2-saturated formation water containing Desulfotomaculum nigrificans, Front. Microbiol. 10 (2019) 1298.
[20] A. Dugstad, Mechanism of Protective Film Formation during Co2 Corrosion of Carbon Steel, CORROSION 98, San Diego, CA, 1998.
[21] E. Chan, D. John, S. Bailey, B. Kinsella, Galvanic Corrosion of Carbon Steel in Carbon Dioxide Caused by Magnetite Paper Number 3092, NACE CORROSION, Las Vegas, NV, 2008.
[22] G.D. Song, S.H. Jeon, Y.H. Son, J.G. Kim, D.H. Hur, Galvanic effect of magnetite on the corrosion behavior of carbon steel in deaerated alkaline solutions under flowing conditions, Corros. Sci. 31 (2018) 71–80.
[23] A.M. Al-Mayouf, Dissolution of magnetite coupled galvanically with iron in environmentally friendly chelant solutions, Corros. Sci. 48 (4) (2006) 898–912.
[24] D. Xu, T. Gu, D.R. Lovley, Microbially mediated metal corrosion, Nat. Rev. Microbiol. (2023) 1–14.
[25] D. Wang, C. Yang, M.A. Saleh, M.D. Alotaibi, M.E. Mohamed, D. Xu, T. Gu, Conductive magnetite nanoparticles considerably accelerated carbon steel corrosion by electroactive Desulfovibrio vulgaris biofilm, Corros. Sci. 205 (2022) 110440.
[26] S. Kato, Microbial extracellular electron transfer and its relevance to iron corrosion, Microb. Biotechnol. 9 (2) (2016) 141–148.
[27] R. Jia, D. Yang, J. Xu, D. Xu, T. Gu, Microbiologically influenced corrosion of C1018 carbon steel by nitrate reducing Pseudomonas aeruginosa biofilm under organic carbon starvation, Corros. Sci. 127 (2017) 1–9.
[28] Y. Jin, E. Zhou, T. Ueki, D. Zhang, Y. Fan, D. Xu, et al., Accelerated microbial corrosion by magnetite and electrically conductive pili through direct Fe0-to-microbe electron transfer, Angew. Chem. Int. Ed. 135 (38) (2023) e202309005.
[29] ASTM G1, Standard Practice for Preparing, Cleaning, and Evaluation Corrosion Test Specimens, ASTM International, West Conshohocken, PA, 2003.
[30] NACE SP0775, Standard Practice Preparation, Installation, Analysis, and Interpretation of Corrosion Coupons in Oilfield Operations, NACE International, Houston, TX, 2013.
[31] K. Dockens, M. Demeter, S. Johnston, S. Leong, Comparison of Planktonic and Sessile Bacteria Counts using ATP and DNA Based Methods, NACE CORROSION, New Orleans, LA, 2017.
[32] S.J. Salgar-Chaparro, L.L. Machuca, K. Lepkova, T. Pojtanabuntoeng, A. Darwin, Investigating the effect of temperature in the community structure of an oilfield microbial consortium, and its impact on corrosion of carbon steel, NACE CORROSION, Nashville, TN, 2019.
[33] N. Da Silva, M.H. Taniwaki, V.C. Junqueira, N. Silveira, M.M. Okazaki, R.A. R. Gomes, Microbiological examination methods of food and water: a laboratory manual, CRC Press, 2018.
[34] S.J. Salgar-Chaparro, L.L. Machuca, Complementary DNA/RNA-based profiling: characterization of corrosive microbial communities and their functional profiles in an oil production facility, Front. Microbiol. 10 (2019), 2587-2587.
[35] S.J. Salgar-Chaparro, K. Lepkova, T. Pojtanabuntoeng, A. Darwin, L.L. Machuca, Microbiologically influenced corrosion as a function of environmental conditions: a laboratory study using oilfield multispecies biofilms, Corros. Sci. 169 (2020) 108595, https://doi.org/10.1016/j.corsci.2020.108595.

[36] Y. Yu, C. Lee, J. Kim, S. Hwang, Group-specific primer and probe sets to detect methanogenic communities using quantitative real-time polymerase chain reaction, Biotechnol. Bioeng. 89 (6) (2005) 670–679.
[37] B.J. Callahan, P.J. McMurdie, M.J. Rosen, A.W. Han, A.J.A. Johnson, S.P. Holmes, DADA2: high-resolution sample inference from Illumina amplicon data, Nat. Methods 13 (2016) 581–583, https://doi.org/10.1038/nmeth.3869.
[38] N.A. Bokulich, B.D. Kaehler, J.R. Rideout, M. Dillon, E. Bolyen, R. Knight, et al., Optimizing taxonomic classification of marker-gene amplicon sequences with QIIME 2's q2-feature-classifier plugin, Microbiome 6 (1) (2018) 1–17.
[39] B. Liu, E. Fan, J. Jia, C. Du, Z. Liu, X. Li, Corrosion mechanism of nitrate reducing bacteria on X80 steel correlated to its intermediate metabolite nitrite, Constr. Build. Mater. 303 (2021) 124454.
[40] W.J. Wiebe, K. Bancroft, Use of the adenylate energy charge ratio to measure growth state of natural microbial communities, PNAS 72 (6) (1975) 2112–2115.
[41] M. Robineau, A. Romaine, R. Sabot, M. Jeannin, V. Deydier, S. Necib, P. Refait, Galvanic corrosion of carbon steel in anoxic conditions at 80° C associated with a heterogeneous magnetite (Fe_3O_4)/mackinawite (FeS) layer, Electrochim. Acta 255 (2017) 274–285.
[42] Y.S. Kim, J.G. Kim, Corrosion behavior of pipeline carbon steel under different iron oxide deposits in the district heating system, Metals 7 (5) (2017) 182.
[43] I. Samusawa, K. Shiotani, Influence of Fe_3O_4 particle size on corrosion of carbon steel under wet/dry cyclic conditions, Mater. Corros. 70 (1) (2019) 57–69.
[44] S. Hassani, J. Huang, A.C. Victor, B. Brown, M. Singer, Inhibited under-deposit CO2 corrosion: small particle silica sand and eicosane paraffin deposits, NACE CORROSION, New Orleans, LA, 2017.
[45] J. Huang, B. Brown, X. Jiang, B. Kinsella, S. Nesid, Internal CO2 Corrosion of Mild Steel Pipelines under Inert Solid Deposits, CORROSION, San Antonio, TX, 2010.
[46] P.K. Baranwal, P.V. Rajaraman, Electrochemical investigation on effect of sodium thiosulfate ($Na_2S_2O_3$) and ammonium chloride (NH_4Cl) on carbon steel corrosion, J. Mater. Res. Technol. 8 (1) (2019) 1366–1378.
[47] H.M. Ezuber, Influence of temperature and thiosulfate on the corrosion behavior of steel in chloride solutions saturated in CO_2, Mater. Des. 30 (9) (2009) 3420–3427.
[48] S. Standlee, K.D. Efird, D. Spiller, Under Deposit Corrosion from Iron Sulfide, NACE CORROSION, Houston.TX, 2011.
[49] M. Robineau, V. Deydier, D. Crusset, A. Bellefleur, D. Neff, E. Vega, et al., Formation of iron sulfides on carbon steel in a specific cement grout designed for radioactive waste repository and associated corrosion mechanisms, Materials 14 (13) (2021) 3563.
[50] S.I. Giannakandropoulou, H. Desjonqueres, C. Wittebroodt, G. Baldacchino, Impact of γ-radiation on carbon steel anaerobic corrosion and H2 production, Radiat. Phys. Chem. 206 (2023) 110742.
[51] N.K. Prasad, A.S. Pathak, S. Kundu, K. Mondal, Influence of deaeration, cl− ion and strong oxidizer on the active behavior of the high phosphorus containing pig iron and subsequent effect on the sacrificial anode behavior, Met. Mater. Int (2021) 1–20.
[52] L. Selwyn, Overview of archaeological iron: the corrosion problem, key factors affecting treatment, and gaps in current knowledge, Proc. Met. (2004) 294–306.
[53] R. Jia, D. Yang, D. Xu, T. Gu, Electron transfer mediators accelerated the microbiologically influence corrosion against carbon steel by nitrate reducing *Pseudomonas aeruginosa* biofilm, Bioelectrochemistry 118 (2017) 38–46.
[54] A. Abdolahi, E. Hamzah, Z. Ibrahim, S. Hashim, Microbially influenced corrosion of steels by *Pseudomonas aeruginosa*, Corros. Rev. 32 (3-4) (2014) 129–141.
[55] L. Huang, Y. Huang, Y. Lou, H. Qian, D. Xu, L. Ma, et al., Pyocyanin-modifying genes phzM and phzS regulated the extracellular electron transfer in microbiologically-influenced corrosion of X80 carbon steel by *Pseudomonas aeruginosa*, Corros. Sci. 164 (2020) 108355.
[56] L. Liang, Y. Ren, Y. Tian, J.A.A. Garcí, P. Zhang, X. Zhu, Role of *Pseudomonas fluorescens* FSYZ01 on the corrosion behavior of Q235B carbon steel in oilfield produced water, Environ. Sci. Pollut. Res. 30 (22) (2023) 62590–62601.
[57] A. Rajasekar, B. Anandkumar, S. Maruthamuthu, Y.P. Ting, P.K. Rahman, Characterization of corrosive bacterial consortia isolated from petroleum-product-transporting pipelines, Appl. Microbiol. Biotechnol. 85 (2010) 1175–1188.
[58] A. Abdolahi, E. Hamzah, Z. Ibrahim, S. Hashim, Localised corrosion of mild steel in presence of *Pseudomonas aeruginosa* biofilm, Corros. Eng. Sci. 50 (7) (2015) 538–546.
[59] R. Jia, D. Yang, J. Xu, D. Xu, T. Gu, Microbiologically influenced corrosion of C1018 carbon steel by nitrate reducing *Pseudomonas aeruginosa* biofilm under organic carbon starvation, Corros. Sci. 127 (2017) 1–9.
[60] Y. Dong, Y.J. Chang, R.A. Sanford, B.W. Fouke, Draft genome sequence of *Tepidibacillus decaturensis* strain Z9, an anaerobic, moderately thermophilic, and heterotrophic bacterium from the deep subsurface of the Illinois Basin, USA, Genome Announcement 4 (2) (2016) 10–1128.
[61] O.A. Podosokorskaya, A.Y. Merkel, S.N. Gavrilov, I. Fedoseev, E.V. Heerden, E. D. Cason, et al., *Tepidibacillus infernus* sp. nov., a moderately thermophilic, selenate-and arsenate-respiring hydrolytic bacterium isolated from a gold mine, and emended description of the genus *Tepidibacillus*, Int. J. Syst. Evol. Microbiol. 66 (8) (2016) 3189–3194.
[62] G.B. Slobodkina, A.N. Panteleeva, N.A. Kostrikina, D.S. Kopitsyn, E.A. Bonch-Osmolovskaya, A.I. Slobodkin, *Tepidibacillus fermentans* gen. nov., sp. nov.: a moderately thermophilic anaerobic and microaerophilic bacterium from an underground gas storage, Extremophiles 17 (2013) 833–839.
[63] X. Chen, T. Han, X. Miao, X. Zhang, L. Zhao, Y. Sun, et al., Ferrihydrite enhanced the electrogenic hydrocarbon degradation in soil microbial electrochemical remediation, J. Chem. Eng. 446 (2022) 136901.
[64] Q. Fu, J. Xu, B. Wei, Q. Qin, L. Gao, Y. Bai, et al., Effect of alternating current and nitrate reducing bacteria on corrosion of X80 pipeline steel in Shenyang soil solution, Eng. Fail. Anal. 129 (2021) 105688.
[65] D. Enning, J. Garrelfs, Corrosion of iron by sulfate-reducing bacteria: new views of an old problem, Appl. Environ. Microbiol. 80 (4) (2014) 1226–1236.
[66] D.Y. Lee, W.C. Kim, J.G. Kim, Effect of nitrite concentration on the corrosion behaviour of carbon steel pipelines in synthetic tap water, Corros. Sci. 64 (2012) 105–114.
[67] S. Lahme, D. Enning, C. Callbeck, D. Menendez-Vega, T. Curtis, I.M. Head, et al., Metabolites of an oil field sulfide-oxidizing, nitrate-reducing *Sulfurimonas* sp. Cause severe corrosion, Appl. Environ. Microbiol. 85 (3) (2019) p. e01891-18.
[68] S. Kawaichi, T. Yamada, A. Umezawa, S.E. McGlynn, T. Suzuki, N. Dohmae, et al., Anodic and cathodic extracellular electron transfer by the filamentous bacterium *Ardenticatena maritima* 110S, Front. Microbiol. 9 (2018) 68.
[69] X. Deng, N. Dohmae, K.H. Nealson, K. Hashimoto, A. Okamoto, Multi-heme cytochromes provide a pathway for survival in energy-limited environments, Sci. Adv. 4 (2) (2018) 5682.
[70] Z. Wang, T. Wang, B. Si, J. Watson, Y. Zhang, Accelerating anaerobic digestion for methane production: potential role of direct interspecies electron transfer, Renew. Sust. Energ. Rev. 145 (2021) 111069.
[71] X. Deng, N. Dohmae, K.H. Nealson, K. Hashimoto, A. Okamoto, Multi-heme cytochromes provide a pathway for survival in energy-limited environments, Sci. Adv. 4 (2) (2018) 5682.
[72] H. Chen, F. Min, X. Hu, D. Ma, Z. Huo, Biochar assists phosphate solubilizing bacteria to resist combined Pb and Cd stress by promoting acid secretion and extracellular electron transfer, J. Hazard. Mater. 452 (2023) 131176.
[73] R.V. Lemos, S. Tsujimura, P. Ledezma, Y. Tokunou, A. Okamoto, S. Freguia, Extracellular electron transfer by *Microcystis aeruginosa* is solely driven by high pH, Bioelectrochemistry 137 (2021) 107637.
[74] W. Dou, J. Liu, W. Cai, D. Wang, R. Jia, S. Chen, T. Gu, Electrochemical investigation of increased carbon steel corrosion via extracellular electron transfer by a sulfate reducing bacterium under carbon source starvation, Corros. Sci. 150 (2019) 258–267.
[75] A.R. Rowe, P. Rajeev, A. Jain, S. Pirbadian, A. Okamoto, J.A. Gralnick, et al., Tracking electron uptake from a cathode into *Shewanella* cells: implications for energy acquisition from solid-substrate electron donors, MBio 9 (2018).
[76] X. Deng, A. Okamoto, Electrode potential dependency of single-cell activity identifies the energetics of slow microbial electron uptake process, Front. Microbiol. 9 (2018) 2744.
[77] P. Liu, P. Liang, Y. Jiang, W. Hao, B. Miao, D. Wang, X. Huang, Stimulated electron transfer inside electroactive biofilm by magnetite for increased performance microbial fuel cell, Appl. Energy 216 (2018) 382–388.
[78] M. Wang, Z. Zhao, Y. Zhang, Magnetite-contained biochar derived from fenton sludge modulated electron transfer of microorganisms in anaerobic digestion, J. Hazard. Mater. 403 (2021) 123972.
[79] Z. Jin, Z. Zhao, Y. Zhang, Potential of direct interspecies electron transfer in synergetic enhancement of methanogenesis and sulfate removal in an up-flow anaerobic sludge blanket reactor with magnetite, Sci. Total Environ. 677 (2019) 299–306.